

# Phase Behavior and Ion Dynamics of Nanoconfined $\text{LiBH}_4$ in Silica

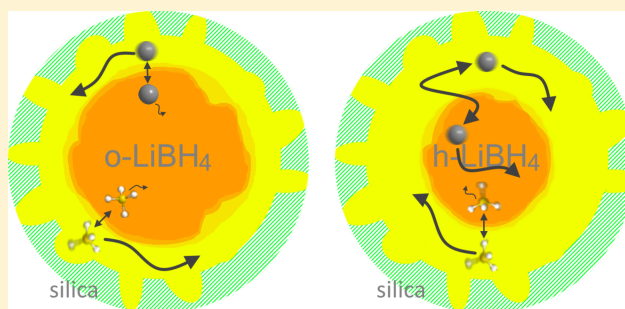
Sander F. H. Lambregts,<sup>†,‡</sup> Ernst R. H. van Eck,<sup>†</sup> Suwarno,<sup>‡</sup> Peter Ngene,<sup>‡</sup> Petra E. de Jongh,<sup>‡</sup> and Arno P. M. Kentgens<sup>\*,†</sup>

<sup>†</sup>Magnetic Resonance Research Center, Institute for Molecules and Materials, Radboud University, Heyendaalseweg 135, 6525 AJ Nijmegen, The Netherlands

<sup>‡</sup>Inorganic Chemistry and Catalysis, Debye Institute for Nanomaterials Science, Utrecht University, Universiteitsweg 99, 3584 CG Utrecht, The Netherlands

## S Supporting Information

**ABSTRACT:** The increasing demand for high capacity yet safe storage of renewable energy calls for the development of all-solid-state batteries. A major hurdle in this development is the identification of new suitable types of solid-state electrolytes. Nanoconfined lithium borohydride is a solid-state electrolyte candidate due to its high lithium-ion mobility at ambient temperatures. The origin of the high lithium-ion mobility is not fully understood, however. We studied nanocomposites of lithium borohydride and nanoporous silica Santa Barbara Amorphous-15 (SBA-15) with different pore sizes, using  $^1\text{H}$ ,  $^6\text{Li}$ , and  $^{11}\text{B}$  solid-state NMR at various temperatures, to get in-depth insights into the phase behavior and ion dynamics of lithium borohydride in the silica pores. The results allow us to formulate a detailed dynamic model for lithium borohydride confined in SBA-15; bulklike  $\text{LiBH}_4$  is separated from the pore walls by an amorphous, highly dynamic  $\text{LiBH}_4$  fraction displaying both  $\text{Li}^+$  and  $\text{BH}_4^-$  diffusion even at ambient temperatures. As shown by  $^{11}\text{B}$  temperature-jump exchange NMR, this dynamic fraction increases as a function of temperature.  $\text{Li}^+$  exchange between the bulklike and “dynamic”  $\text{LiBH}_4$  fraction is slow at ambient temperatures, but at elevated temperatures ( $\geq 90^\circ\text{C}$ ), above the phase transition of the bulklike fraction, lithium ions rapidly diffuse through both  $\text{LiBH}_4$  fractions and exchange between these confined fractions at rates approaching the megahertz time scale.



## INTRODUCTION

Rechargeable batteries are crucial in modern-day society. Unfortunately, current lithium-ion batteries have a low energy density, making them suboptimal for high-demand applications, such as powering electric cars or intermediate storage of energy from renewable sources. The development of new battery materials is crucial to make this possible.

A lithium-ion battery consists of two electrodes separated by an electrolyte. The purpose of the electrolyte is to transport the ionic charge carriers,  $\text{Li}^+$ , while preventing electron transfer. In terms of energy density, the most ideal anode material is metallic lithium. However, the currently used electrolyte materials, lithium salts in organic solvents, are not compatible with metallic lithium.<sup>1–3</sup> Solid-state electrolytes are considered a promising alternative to overcome these stability problems. Furthermore, solid-state electrolytes will reduce the safety issues (i.e., instability and flammability) associated with present electrolytes.<sup>4</sup>

A specific class of materials, the complex metal hydrides, possess high ionic conductivities and are compatible with lithium metal, by forming a stable interface layer.<sup>5–7</sup> One of those materials, lithium borohydride ( $\text{LiBH}_4$ ), is a promising electrolyte candidate for use in an all-solid-state battery.<sup>8</sup> Bulk  $\text{LiBH}_4$  has been extensively studied. It undergoes a phase

transition from an orthorhombic to a hexagonal crystal lattice at around  $110^\circ\text{C}$  at standard pressures.<sup>9</sup> In the high-temperature phase, the  $\text{Li}^+$  ions diffuse rapidly through the hexagonal crystal lattice, resulting in a high ionic conductivity. However, the conductivity is low in the orthorhombic phase, where only slow hopping of  $\text{Li}^+$  is observed, making bulk  $\text{LiBH}_4$  unsuitable for commercial use in batteries.<sup>8</sup>

To be useful as an electrolyte in batteries for commercial applications, a high ionic conductivity of at least  $1\text{ mS/cm}$  is desired at ambient conditions.<sup>3</sup> To achieve this, a phase with a  $\text{Li}^+$  mobility comparable to that of the high-temperature phase of  $\text{LiBH}_4$  must be stabilized at room temperature. Various chemical modifications to achieve this have successfully been employed, at the cost of (electro)chemical stability.<sup>10–14</sup>

Another approach to modify the properties of  $\text{LiBH}_4$  is by confinement in nanoporous hosts,<sup>15–17</sup> which was shown to improve the  $\text{Li}^+$  mobility at room temperature by several orders of magnitude.<sup>18</sup> Confinement leads to a decrease of the long-range order of the confined material.<sup>16</sup> Further effects may result from interactions with the scaffold.<sup>19</sup> This is

Received: July 8, 2019

Revised: September 8, 2019

Published: September 30, 2019



Table 1. Properties of the LiBH<sub>4</sub>/SiO<sub>2</sub> Nanocomposites and Their SBA-15 Silica Scaffolds<sup>a</sup>

sample	SBA-15 silica scaffold				nanocomposite	
	$T_{ht}$ (°C)	$d_{BJH}$ (nm)	$S_{BET}$ (m <sup>2</sup> /g)	$V_{pore}$ (meso/micro)	pores filled (%)	oxidized (%)
MI-MS-8	100	8	695	0.93 mL/g (84/9%)	90 (85)	5
MI-MS-7	80	7	800	0.80 mL/g (76/20%)	90 (89)	6
MI-MS-5	40	5	671	0.51 mL/g (66/32%)	90 (93)	18

<sup>a</sup> $T_{ht}$  is the hydrothermal treatment temperature,  $d_{BJH}$  the pore diameter,  $S_{BET}$  the surface area, and  $V_{pore}$  the pore volume (between brackets the relative amount of meso- and micropores as determined using the Harkins–Jura reference isotherm,<sup>31</sup> excluding the interparticle volume). Pores filled is the hypothetical and, between brackets, experimentally determined fraction of pores that is filled with LiBH<sub>4</sub>. Oxidized is the fraction of the boron atoms corresponding to oxidation products of LiBH<sub>4</sub>.

corroborated by the observation of the increased mobility of a small fraction of the lithium ions in composites prepared by mechanical milling of LiBH<sub>4</sub> with silicas or aluminas.<sup>20,21</sup> Das et al. have shown that nanoconfined LiBH<sub>4</sub> can be used in an all-solid-state battery, revealing a good cycling stability and high capacity of this battery.<sup>7,22</sup> The exact origin of the increase in ionic conductivity is still not known, although it is shown to be an interface effect.<sup>19–21</sup>

One of the most remarkable features of lithium borohydride nanocomposites is that the confined LiBH<sub>4</sub> is divided into two distinct fractions. One fraction, within a few nanometers of the oxide interface, displays high ionic mobility at room temperature, whereas the other expresses more bulklike behavior, including a structural phase transition.<sup>18,19,23,24</sup> However, how these fractions with different Li<sup>+</sup> mobilities influence the overall ionic conductivity of the nanocomposite is not yet understood. Here we study the temperature behavior of lithium borohydride in these two fractions, primarily focusing on the local environment and dynamics in these lithium borohydride fractions.

Solid-state NMR, being sensitive to both the local environment of nuclei and their dynamics, is a versatile tool for studying complex dynamic systems such as nanoconfined LiBH<sub>4</sub>.<sup>25</sup> NMR spectra of quadrupolar nuclei such as <sup>11</sup>B and <sup>7</sup>Li, both spin 3/2, display quadrupolar line shapes, which are strongly affected by the local environment of the nucleus. In the case of relatively small quadrupolar interactions, as for <sup>7</sup>Li, this is mainly manifested in the width and shapes of the  $\pm 3/2 \leftrightarrow \pm 1/2$  satellite transitions. Apart from the NMR line shapes of quadrupolar nuclei, the line shapes and widths of all relevant nuclei (<sup>1</sup>H, <sup>6</sup>Li, <sup>7</sup>Li, and <sup>11</sup>B) are influenced by dynamics. In a situation where all atoms move slowly (on the NMR time scale), broad lines are typically observed due to the chemical shift anisotropy, quadrupolar interactions, and/or dipolar interactions between nuclei. On the other hand, if the motion is very fast and the relative orientation of the nuclei changes continuously, the anisotropic NMR interactions will be (partially) averaged. In this study, we combine the structural sensitivity of NMR via the quadrupolar interaction of <sup>7</sup>Li with the sensitivity toward dynamics of <sup>1</sup>H, <sup>7</sup>Li, and <sup>11</sup>B NMR to elucidate the remarkable two-component behavior of nanoconfined LiBH<sub>4</sub>.

## ■ EXPERIMENTAL SECTION

**Sample Preparation.** Bulk LiBH<sub>4</sub> was purchased from Acros Organics (95% pure). The Santa Barbara Amorphous-15 (SBA-15) silica scaffolds were synthesized according to the procedure used by Eggenhuisen et al.<sup>26</sup> The structural properties of the scaffolds are summarized in Table 1. The pore size was varied by changing the hydrothermal treatment temperature.<sup>27</sup> The surface area,<sup>28</sup> pore diameter,<sup>29,30</sup> and

total-, meso-, and micropore volumes<sup>31</sup> of the calcined SBA-15 silicas were determined using N<sub>2</sub>-physisorption, measured on a Micromeritics TriStar surface area and porosity analyzer. The pore size distribution is shown in Figure S1, and a comparison of the pore diameters obtained via the classical method of Barrett, Joyner, and Halenda (BJH-model) and density functional theory (DFT) is shown in Table S1. Typically, DFT calculations predict slightly larger pore sizes.<sup>32,33</sup> The mesoporous silica scaffolds are named MS-*d*, where *d* denotes the BJH pore diameter in nanometers.

Infiltration of the silica with LiBH<sub>4</sub> was done according to the procedure of Ngene et al.<sup>16</sup> The amount of LiBH<sub>4</sub> used corresponds to 90% of the pore volume of the silicas (25, 33, or 36 wt %). Prior to melt-infiltration, the SBA-15 was dried for several hours at 500 °C in a flow of inert gas. Successful infiltration was confirmed using calorimetry (Figure S2) and X-ray diffraction (XRD) (Figure S3).<sup>18</sup> <sup>11</sup>B magic-angle spinning (MAS) NMR (Figure S4) proved to be a sensitive probe for oxidation of the samples and was used to quantify the amount of oxidized boron species. The results are listed in Table 1. The melt-infiltrated samples are denoted MI-[scaffold]. The nanocomposites were stored in Ar- or N<sub>2</sub>-filled gloveboxes with O<sub>2</sub> and H<sub>2</sub>O levels typically below 1 ppm.

In between experiments, samples were stored in a glovebox for extended periods of time. Prior to the novel experiment series, samples were checked for potential oxidation using <sup>11</sup>B MAS NMR, whereas <sup>6</sup>Li MAS NMR was performed to verify the presence of two different lithium fractions at room temperature. Even after storage for more than a year, no significant changes were observed, indicating the remarkable stability of the samples when stored in an inert atmosphere.

**Solid-State NMR.** Solid-state NMR experiments were performed on 7.05, 9.39, and 20.0 T Varian VNMR spectrometers using 5.0 mm static Bruker, Chemagnetics APEX 3.2 mm MAS, and 1.2 and 4.0 mm Varian T3 MAS probes, respectively. Temperatures were calibrated using liquid ethylene glycol or solid lead(II) nitrate at 2 kHz MAS rate.<sup>34–36</sup> Frictional heating due to MAS and associated temperature gradients in the sample<sup>37,38</sup> have not been taken into account, but we estimate this deviation to be less than 10 °C under the conditions used in this study. Experiments were performed under a flow of nitrogen due to the reactive nature of the samples.

<sup>1</sup>H single-pulse excitation (SPE) experiments were performed using 90° pulses at a radio frequency (RF) field strength of 80–90 kHz. <sup>6</sup>Li SPE experiments employed 50–60 kHz RF field applying 90° pulses to excite the spins. <sup>7</sup>Li and <sup>11</sup>B SPE experiments were performed using an RF field strength of 80–90 kHz and flip angles of 30° or less to warrant a quantitative evaluation of the spectra.<sup>39</sup> Solid echo experiments<sup>40</sup> were performed using 90° pulses. SPINAL<sup>41</sup>

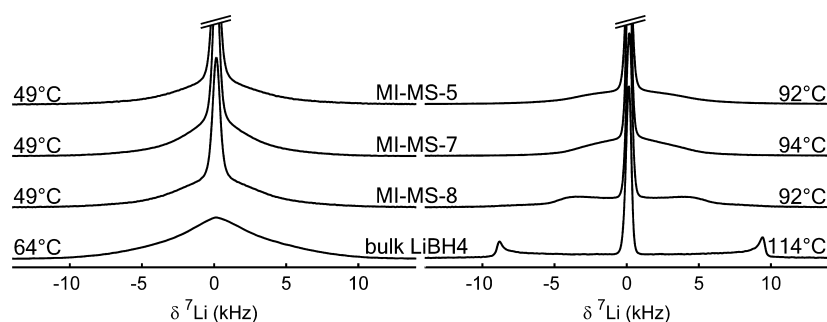


**Figure 1.** Normalized  $^7\text{Li}$  NMR spectra of bulk  $\text{LiBH}_4$  and  $\text{LiBH}_4$  confined in 5–8 nm silica pores, at temperatures below (left) and above (right) their respective structural phase transition temperatures. These static solid echo spectra were acquired at 9.4 T. Spectra of the nanocomposites were obtained going from high to low temperature. Additional spectra acquired at different temperatures can be found in Figures S5 and S6.

$^1\text{H}$  decoupling at RF field strengths of 60–110 kHz was applied in  $^6\text{Li}$ ,  $^7\text{Li}$ , and  $^{11}\text{B}$  SPE or solid echo experiments, except for  $^6\text{Li}$  MAS experiments, where RF field strengths of 10–20 kHz were employed. The delay between pulses in echo experiments was 14–17  $\mu\text{s}$ . The contribution of extraporous bulk  $\text{LiBH}_4$  to the spectra was reduced by waiting for only three  $T_1$  of the confined  $\text{LiBH}_4$  fractions between scans; the  $T_1$  of bulk  $\text{LiBH}_4$  is an order of magnitude longer than the observed  $T_1$  of confined material. Saturation recovery experiments<sup>42</sup> were used to determine the (effective) spin–lattice relaxation times ( $T_1$ ). Two-dimensional (2-D)  $^{11}\text{B}$  exchange spectroscopy<sup>43</sup> (EXSY) and  $\{^1\text{H}\}^{11}\text{B}$  heteronuclear correlation<sup>44</sup> (HETCOR) experiments were performed under fast MAS using 150 kHz proton decoupling during acquisition and, in the EXSY experiments, during the evolution period. The cross-polarization contact time in the HETCOR experiment was 800  $\mu\text{s}$ . A temperature jump was induced by RF heating (by dissipation of adsorbed energy via dielectric losses in the samples)<sup>45</sup> in an EXSY experiment by applying continuous-wave irradiation at an RF field strength of 150 kHz on the proton channel during the 45 ms mixing time.

All spectra were processed using the Matlab toolbox matNMR.<sup>46</sup> The spectra were externally referenced to tetramethylsilane, lithium chloride solution, or solid adamantane, using the frequency ratios, if needed.<sup>47,48</sup> ITMPM linear backward prediction,<sup>49</sup> as implemented in matNMR, was used for processing static  $^1\text{H}$  and  $^7\text{Li}$  and MAS  $^{11}\text{B}$  SPE spectra to compensate for line distortions due to the receiver dead time. Simulations of quadrupolar line shapes were performed using SIMPSON.<sup>50</sup>

## RESULTS

**Phase Behavior of  $\text{LiBH}_4/\text{SiO}_2$  Nanocomposites.**  $^{6,7}\text{Li}$  NMR. We first discuss the structural behavior of bulk  $\text{LiBH}_4$ . Figure 1 (bottom spectra) shows  $^7\text{Li}$  spectra of bulk  $\text{LiBH}_4$ . The spectrum obtained at 64  $^\circ\text{C}$ , showing the line shape of the orthorhombic low-temperature phase o- $\text{LiBH}_4$ , consists of a single, broad peak. At 114  $^\circ\text{C}$ , above the structural phase transition temperature ( $T \approx 110$   $^\circ\text{C}$ ), the spectrum of hexagonal (h)- $\text{LiBH}_4$  consists of a narrow central peak ( $-1/2 \leftrightarrow 1/2$  spin transition) and a pattern characteristic for the quadrupolar satellite transitions ( $\pm 3/2 \leftrightarrow \pm 1/2$ ) (Figure 1). The broad line shape in the low-temperature phase is the result of dipolar interactions of  $\text{Li}^+$  ions with nearby nuclei, which exceed the magnitude of the quadrupolar interaction in that phase ( $C_Q \approx 16$  kHz,  $\eta \approx 0.8$ ).<sup>51</sup> In the high-temperature phase, the high  $\text{Li}^+$  mobility effectively

removes the dipolar interactions between neighboring spins, resulting in a very narrow line for the central transition. However, this motion does not average the quadrupolar interaction ( $C_Q \approx 37$  kHz,  $\eta \approx 0$ ). The rapid dynamics of the lithium ions is restricted to hopping between crystal lattice sites such that the line shapes of the satellite transitions result from an average over the quadrupolar interactions of the sites visited during the fast ion hopping process. NMR relaxometry showed that the lithium motion in the high-temperature phase is two-dimensional, restricted to planes in the crystal lattice.<sup>52</sup>

Nanostructuring of  $\text{LiBH}_4$  in silica has been found to be a very efficient method to increase the lithium mobility at room temperature.<sup>18</sup> To gain more insights into the effect of confinement, and/or the influence of the  $\text{LiBH}_4$ – $\text{SiO}_2$  interface, we study composites of  $\text{LiBH}_4$  confined in silica (SBA-15) with pore diameters of 5, 7, and 8 nm. The synthesis and characterization of the nanocomposites are described in the Experimental Section.

Suwarno et al.<sup>19</sup> determined the thermal behavior of this type of nanocomposites and bulk  $\text{LiBH}_4$  by differential scanning calorimetry (DSC). As reproduced in Figure S2, for bulk  $\text{LiBH}_4$ , only a single endothermic peak near 110  $^\circ\text{C}$ , corresponding to the structural phase transition of  $\text{LiBH}_4$ , is observed. The DSC curves of the nanocomposites show broad endothermic peaks between 70 and 100  $^\circ\text{C}$ . The temperature of the structural phase transition of  $\text{LiBH}_4$  in the core of the pores decreases upon confinement.<sup>18,19,53</sup> Hence, the broad, endothermic peak is ascribed to a structural phase transition of confined  $\text{LiBH}_4$ .

Figure 1 shows the  $^7\text{Li}$  spectra of  $\text{LiBH}_4$  confined in silica nanopores at about 93  $^\circ\text{C}$ . This is above the structural phase transition temperature of confined  $\text{LiBH}_4$  as observed by DSC, but below the transition temperature of bulk  $\text{LiBH}_4$ . Clearly, the appearance of the spectra differs from that of the spectra of bulk  $\text{LiBH}_4$  in the high- or low-temperature phase. A previous NMR investigation of a  $\text{LiBH}_4/\text{SiO}_2$  nanocomposite revealed a complicated  $^7\text{Li}$  line shape at 120  $^\circ\text{C}$ , which resembled neither the high- or low-temperature phase of bulk  $\text{LiBH}_4$  nor the line shape of confined  $\text{LiBH}_4$  near ambient conditions.<sup>18</sup>

The spectrum of MI-MS-8 at 92  $^\circ\text{C}$  consists of a narrow central peak and a broad line shape, which shows features resembling the satellite transitions of a quadrupolar nucleus (with a  $C_Q \approx 18$  kHz and  $\eta \approx 0$ , Figure S7), meaning that the local environment of the lithium ions is relatively ordered. The line shape nevertheless differs from the quadrupolar line shape of the high-temperature phase of bulk  $\text{LiBH}_4$ , which has a quadrupolar interaction that is twice as large. In addition, the features of the line shape of the nanocomposite are somewhat



smear out compared to the sharp, well-defined, features observed for bulk  $\text{LiBH}_4$ .

The line shape in the spectrum of MI-MS-7 at 94 °C differs from that in the spectrum of MI-MS-8. This spectrum again consists of a narrow and a broad line shape. However, in this sample, the broad line shape is featureless, rather than resembling a distinct quadrupolar powder pattern. The same is true for MI-MS-5, at 92 °C. A gradual disappearance of the quadrupolar features of the broad component with decreasing pore size can have structural or dynamic origins (vide infra).

The chemical shift range of lithium is very small, making it generally not feasible to distinguish multiple lithium components based on their  $^7\text{Li}$  chemical shift alone. Figure S8 shows the  $^7\text{Li}$  magic-angle spinning (MAS) NMR spectra of MI-MS-7 at 74, 94, and 128 °C. The spectra at 74 and 94 °C, below and above the phase transition temperature of nanoconfined  $\text{LiBH}_4$ , respectively, each consist of a single peak. Only at 128 °C, above the structural phase transition of bulk  $\text{LiBH}_4$ , an additional small peak becomes visible. We assign this peak to extraporous hexagonal bulk  $\text{LiBH}_4$ .

To determine whether the broad component in  $^7\text{Li}$  spectra corresponds to a second lithium species,  $^6\text{Li}$  NMR is studied. The quadrupole moment of  $^6\text{Li}$  is about 50 times smaller with respect to  $^7\text{Li}$ , e.g., the quadrupole moment of bulk h- $\text{LiBH}_4$  (approximately 37 kHz in  $^7\text{Li}$  NMR) is only about 770 Hz in  $^6\text{Li}$  NMR<sup>52</sup> corresponding to 17 ppm at 7 T. Therefore, quadrupolar interactions can still contribute to the static line width in  $^6\text{Li}$  spectra but can easily be spun out in MAS spectra. Figure 2 shows the static  $^6\text{Li}$  spectrum of MI-MS-5 at room

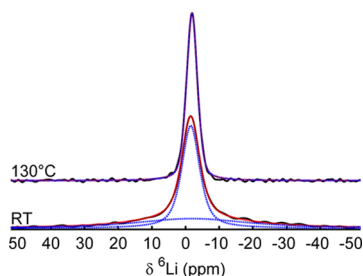


**Figure 2.**  $^6\text{Li}$  static SPE NMR spectra of MI-MS-5 at two temperatures. The spectra were acquired at 7.05 T. Deconvolution of these spectra is shown with dotted lines (blue for the individual peaks, red for the sum). The relative integrals at room temperature are 70 and 30% ( $\pm 10\%$ ) for the narrow and broad components, respectively.

temperature and 130 °C. At 130 °C, only a single, narrow peak (full width at half-maximum of 4 ppm) is visible in the spectrum, in contrast to the  $^7\text{Li}$  spectra of this nanocomposite at similar temperatures, shown in Figures 1 and S6, which consist of a narrow peak and a broad featureless peak. The absence of a broad peak in  $^6\text{Li}$  spectra at 130 °C reveals that, given the different quadrupole moments of the lithium isotopes, the broad line shape in  $^7\text{Li}$  spectra at elevated temperatures can be exclusively assigned to quadrupolar satellite transitions, rather than an additional lithium site. This suggests that all lithium ions of confined lithium borohydride are mobile and largely indistinguishable on the NMR time scale at temperatures above the structural phase transition of the confined material. This is corroborated by the single narrow line in the  $^6\text{Li}$  MAS spectrum of MI-MS-7 above the phase transition temperature (Figure 3).

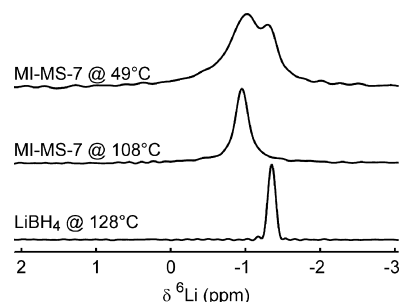


**Figure 3.**  $^6\text{Li}$  MAS SPE NMR spectra of MI-MS-7. There are two distinct lithium signals with different chemical shifts below the DSC phase transition temperature (top spectrum) and a single lithium signal above the phase transition temperature (middle trace). This signal clearly differs from that of the bulk h- $\text{LiBH}_4$  (bottom spectrum).

We now focus on the nanocomposites at temperatures below the phase transition observed by DSC. Each of the  $^7\text{Li}$  spectra of the nanocomposites at 49 °C (Figure 1) consists of two overlapping peaks, a broad and a narrow one. The broad peak was shown to originate from quadrupolar satellite transitions at elevated temperatures. The static  $^6\text{Li}$  spectrum of MI-MS-5 at room temperature, shown in Figure 2, also displays a broad and a narrow peak.  $^6\text{Li}$  MAS NMR spectra of MI-MS-7, as shown in Figure 3, reveal the presence of two lithium fractions with slightly different chemical shifts. One fraction is located at the same chemical shift as bulk  $\text{LiBH}_4$  (for which the lithium chemical shift is nearly temperature independent<sup>51</sup>). The other fraction resonates downfield of bulk  $\text{LiBH}_4$ . Hence, the broad peak observed in  $^7\text{Li}$  spectra obtained at near-ambient temperatures cannot be attributed to the quadrupolar interaction alone. Therefore, the broad and narrow components in the static lithium spectra are not merely due to a distribution in correlation times but due to the coexistence of two separate fractions with slightly different lithium environments, as became evident from the  $^6\text{Li}$  MAS NMR spectra.

The difference in the line width of the two lithium peaks at near-ambient conditions, shown in Figures 1 and 2, indicates that the two lithium species display significantly different mobilities, with the narrow peak corresponding to the most mobile species, in line with earlier studies.<sup>17,18,23,24</sup> In view of this difference in mobility, we will refer to the separate fractions as the dynamic and less-dynamic fraction throughout the article.

In summary, both the difference in the chemical shift and the difference in the quadrupolar interaction show that nanoconfined  $\text{LiBH}_4$  differs from bulk  $\text{LiBH}_4$ . It is furthermore clear that there are two different fractions of  $\text{LiBH}_4$  in the pores at near-ambient temperatures, whereas all lithium is highly mobile and not further distinguishable by NMR at elevated temperatures.

**$^1\text{H}$  NMR.** As the quadrupolar interaction of  $^7\text{Li}$  complicates a quantitative analysis of the ratios of the lithium fractions, we resort to  $^1\text{H}$  NMR.  $^1\text{H}$  NMR spectra of the borohydride anions also reveal the presence of less- and more-dynamic fractions (see Figure S9). Quantitative analysis of these spectra is straightforward, giving the  $\text{LiBH}_4$  distributions in the sample, with the mobility of the  $\text{BH}_4^-$  fractions guiding the analysis.

Figure 4 shows the relative intensities of the narrow and broad components of the  $\text{LiBH}_4/\text{SiO}_2$  nanocomposites as a

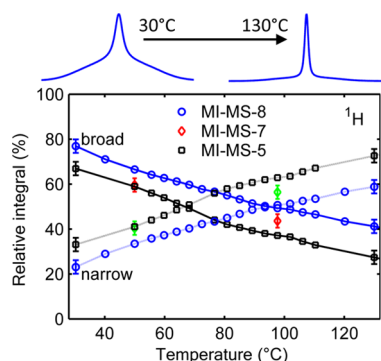


**Figure 4.** Relative integrals of the two  $^1\text{H}$  fractions in static SPE spectra as a function of temperature. The broad component is indicated by solid lines and the narrow component by dashed lines. The error is indicated only at some data points for clarity, but it is similar at all temperatures. The corresponding  $^1\text{H}$  spectra of MI-MS-8 at 30 and 130  $^\circ\text{C}$  are shown above the graph.

function of temperature. The relative amounts were calculated from the integrals of the broad and narrow components by deconvolution of static  $^1\text{H}$  spectra (Figure S9). Two important trends can be derived. First, the relative amount of the dynamic fraction (narrow peak) of  $\text{LiBH}_4$  increases with increasing temperature, and consequently, the relative abundance of the less-dynamic fraction (broad peak) is more abundant in nanocomposites with larger pore sizes, at any given temperature.

The dependence of the  $\text{LiBH}_4$  fractions on the diameter of the pores fits well with the proposed core-shell model for  $\text{LiBH}_4$  confined in nanoporous scaffolds.<sup>23,24</sup> In this model, highly mobile  $\text{LiBH}_4$  is present near the pore wall, whereas the less-mobile  $\text{LiBH}_4$  is located in the core of the silica pores. Assuming cylindrical pores with radius  $r_p$  and a uniform  $\text{LiBH}_4$  density, the theoretical wall fraction thickness  $t$  corresponding to the relative integrals can be estimated via

$$t = r_p(1 - \sqrt{f_{\text{less-dynamic}}}) \quad (1)$$

where  $f_{\text{less-dynamic}}$  is the fraction of less-dynamic  $\text{LiBH}_4$ . The data presented here would correspond to a dynamic  $\text{LiBH}_4$  layer thickness of about 0.5 nm at 30  $^\circ\text{C}$  to a thickness of about 1.2 nm at 110  $^\circ\text{C}$ , as shown in Figure S10. Density functional theory calculations of the pore size<sup>30</sup> (Table S1) predict pore radii and therefore layer thicknesses  $t$  of the wall fraction of about 30% larger size (about 0.6 and 1.5 nm at 30 and 110  $^\circ\text{C}$ , respectively).

Using calorimetry, a (temperature-independent) layer thickness of  $\sim 1.9$  nm was found for the highly mobile  $\text{LiBH}_4$  on SBA-15 pore walls.<sup>19</sup> This is much larger than we observe on the basis of NMR spectra (Figure S10). The differences between these thicknesses may stem from the assumption in calorimetry that the phase transition enthalpy of confined  $\text{LiBH}_4$  is equal to that of bulk  $\text{LiBH}_4$ . Our experiments, however, show a difference in the lithium environment of bulk and nanoconfined  $\text{LiBH}_4$ . Moreover, different methods have different sensitivities toward dynamics in the sample. Finally, it is worth remembering that SBA-15 has very corrugated pore walls; therefore, a description using cylindrical pores is an oversimplification.<sup>54</sup>

The distribution of the fractions obtained via  $^1\text{H}$  NMR depends strongly on the motion of the anions. As the borohydride ions can undergo both translational and rotational

motions, narrowing of the broad line may result from the rotational motion of the borohydride ions.<sup>55</sup> Jimura et al.<sup>56</sup> calculated the  $^1\text{H}$  line widths of  $\text{LiBH}_4$  under various types of motion. In the absence of any motion, the  $^1\text{H}$  line width of bulk  $\text{LiBH}_4$  would be 69 kHz or larger. The isotropic rotation of the  $\text{BH}_4^-$  units reduces this width to 24 and 23 kHz in the low- and high-temperature phases of  $\text{LiBH}_4$ , respectively. For bulk  $\text{LiBH}_4$ , this line width is already observed experimentally at  $-100$   $^\circ\text{C}$ , meaning that the  $\text{BH}_4^-$  units rotate rapidly at that temperature. Additional line narrowing in  $^1\text{H}$  spectra of bulk  $\text{LiBH}_4$  is not observed until temperatures above 150  $^\circ\text{C}$ , where the translational motion of  $\text{BH}_4^-$  becomes significant.<sup>57</sup> The  $^1\text{H}$  line widths of our nanocomposites at 30  $^\circ\text{C}$  are about 21 and 4 kHz for the less-dynamic and dynamic fractions, respectively. Hence, in both fractions, the  $\text{BH}_4^-$  ions rotate isotropically at 30  $^\circ\text{C}$ .  $\text{BH}_4^-$  diffusion is responsible for the narrowing of the line width to 4 kHz in the dynamic fraction, whereas this translational motion plays a minor role in the less-dynamic fraction.

For comparison, the relative integrals of the narrow and broad  $^7\text{Li}$  resonances were determined as well (Figure S11). Near 30  $^\circ\text{C}$ , the intensity ratios of the broad and narrow components as determined via the  $^1\text{H}$  and  $^7\text{Li}$  NMR spectra are similar. This similarity indicates that the contribution of any residual silanol ( $\text{SiOH}$ ) groups of the pure silica after melt-infiltration is very small, strengthening the validity of using  $^1\text{H}$  NMR for quantification. The ratios obtained via  $^7\text{Li}$  and  $^1\text{H}$  NMR start to diverge with increasing temperature. At the phase transition temperature of the confined phase, the broad to narrow ratio for  $^7\text{Li}$  converges to a 6:4 ratio. This ratio corresponds to the theoretical ratio<sup>58</sup> expected for the satellite and central transitions due to the quadrupolar interaction of a spin 3/2 nucleus. This implies that we indeed observe a single dynamic lithium fraction above this phase transition temperature as discussed above, whereas the proton spectra show there are still two fractions of  $\text{BH}_4^-$  units with very different mobilities.

The results presented in this section imply that the thickness of the  $\text{LiBH}_4$  fraction with highly mobile ions near the walls of the silica pores increases with temperature. This change is continuous with temperature for the borohydride ions, whereas for the lithium ions, the distinction between the fractions vanishes at elevated temperatures.

**$^{11}\text{B}$  NMR.** To obtain additional information about the dynamics of the ions in the  $\text{LiBH}_4$  fractions, we focused on the borohydride ions using  $^{11}\text{B}$  MAS NMR. Bulk  $\text{LiBH}_4$  consists entirely of magnetically identical  $\text{BH}_4^-$  ions. Therefore, the  $^{11}\text{B}$  spectrum of bulk  $\text{LiBH}_4$  consists of a single peak, located at  $-41$  ppm.<sup>51</sup>

$^{11}\text{B}$  spectra of nanoconfined  $\text{LiBH}_4$ , as shown in Figure S12, consist of two distinct peaks. This shows the simultaneous existence of two magnetically different boron species. The upfield peak ( $-41.3$  ppm) has the same chemical shift as bulk  $\text{LiBH}_4$ . The other peak is shifted downfield by about 1 ppm ( $-40.5$  ppm) and is narrower than the upfield peak. The presence of two distinct boron peaks with different mobilities was observed before by Verkuijlen et al. in  $\text{LiBH}_4/\text{SiO}_2$  nanocomposites.<sup>17</sup> They proved that the dynamic boron species also consists of a boron atom with four covalently bound hydrogen atoms, i.e.,  $\text{BH}_4^-$ , instead of a chemically different boron compound. A difference in the mobility of an otherwise chemically identical compound does not result in a

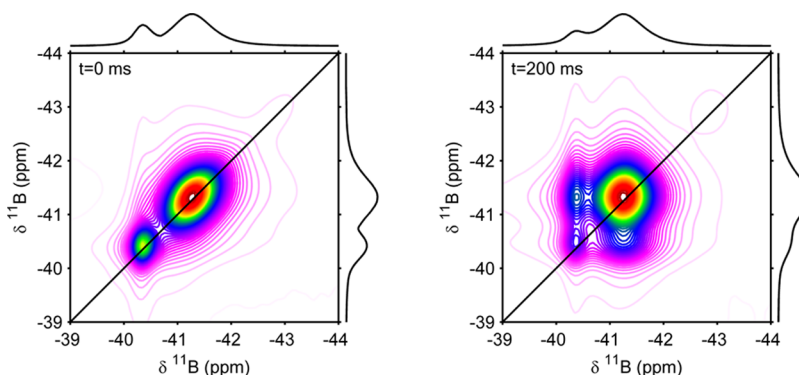


**Figure 5.** Homonuclear  $^{11}\text{B}$  two-dimensional exchange spectroscopy (EXSY) experiment of MI-MS-8 with mixing times of 0 (left) and 200 ms (right), carried out at 20.0 T under 40 kHz MAS at 50 °C. Skyline projections are shown at the sides of the spectra.

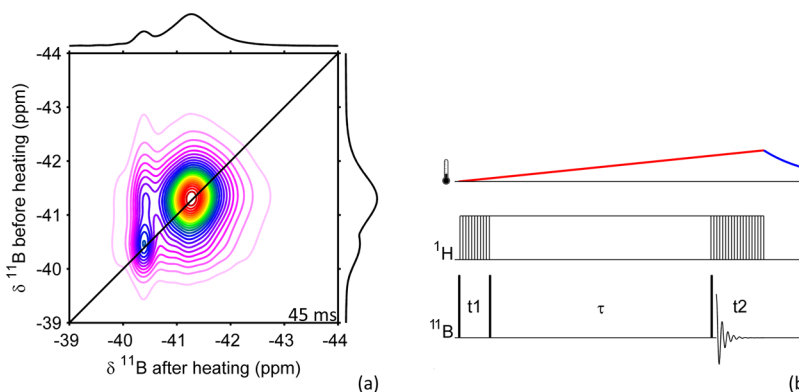


**Figure 6.** (a) Two-dimensional homonuclear  $^{11}\text{B}$  exchange spectrum of MI-MS-8 and (b) pulse sequence, showing the timing of pulses and the expected temperature profile of the sample. Strong radio frequency irradiation was applied on the proton channel during the exchange time  $\tau$  of 45 ms to induce a temperature increase. The spectrum was recorded at 20.0 T under 40 kHz magic-angle spinning at a set temperature of 50 °C. Skyline projections are shown at the sides of the spectrum.

chemical shift difference. Therefore, the local environment of the borohydride anions must be (slightly) different.

The chemical shift separation between the two  $^{11}\text{B}$  components exists over the entire temperature range studied (30–130 °C). As shown in Figure S13, the ratios of the two components change in favor of the downfield component with increasing temperature. These ratios exhibit the same behavior as the ratios obtained from the analysis of the  $^1\text{H}$  spectra (Figure 4). The separation of the peaks confirms that the two boron resonances reflect the presence of  $\text{BH}_4^-$  in either the dynamic or less-dynamic fraction of nanoconfined  $\text{LiBH}_4$ .

An  $^{11}\text{B}$ – $^1\text{H}$  heteronuclear correlation spectrum (Figure S14) shows the chemical shifts of the two boron species along the horizontal axis, separated by about 1 ppm. The chemical shifts of the corresponding proton species are shown along the vertical axis. The chemical shifts of the two  $^1\text{H}$  peaks are identical, to an accuracy of at least 0.3 ppm. Łodźiana and Błoński have proposed a theoretical model for the distribution of  $\text{LiBH}_4$  throughout the pores of nanoporous carbon.<sup>59</sup> In this model, confined lithium borohydride is ordered in one-dimensional chains, two-dimensional ribbons, three-dimensional (3-D) chains, and bulk. For each of the components, they calculated the expected  $^1\text{H}$  and  $^{11}\text{B}$  chemical shifts. In their theoretical model, the only components with an  $^{11}\text{B}$  chemical shift downfield of bulk  $\text{LiBH}_4$  and a  $^1\text{H}$  chemical shift similar to bulk are the proposed one-dimensional chains of  $\text{LiBH}_4$ , although the majority of the calculated shifts of such a component deviates more than 0.3 ppm from bulk  $\text{LiBH}_4$ . Our

spectra do not show evidence for 2-D ribbons ( $\delta_{\text{H}}^{\text{calc}} \ll \delta_{\text{H,bulk}}^{\text{calc}}$ ) or 3-D chains ( $\delta_{\text{B,H}}^{\text{calc}} \ll \delta_{\text{B,bulk}}^{\text{calc}}$ ). We conclude that their model cannot be applied directly to  $\text{LiBH}_4/\text{SiO}_2$  nanocomposites.

**$\text{BH}_4^-$  Exchange.** An important implication from the changing ratios of the boron and proton fractions as a function of temperature is that the dynamic and less-dynamic fractions of  $\text{LiBH}_4$  interconvert. Such a process where, upon heating, less-dynamic  $\text{LiBH}_4$  becomes part of the dynamic fraction has been observed before.<sup>23,60</sup> However, in a  $\text{LiBH}_4/\text{SiO}_2$  nanocomposite with a silica pore diameter of 2 nm, no interconversion of the more- and less-dynamic phases was observed as a function of temperature.<sup>17</sup> It should be noted that the silica used in that study [Mobil Composition of Matter 41 (MCM-41)] differed from the one used in the present investigation (SBA-15).

Figure 5 shows homonuclear  $^{11}\text{B}$  exchange spectra with mixing times of 0 and 200 ms, recorded at 50 °C. The two boron species can be clearly distinguished on the diagonal. During a mixing time of 200 ms, slow exchange of the  $\text{BH}_4^-$  ions between the two fractions occurs on the millisecond time scale, as is clear from the two cross-peaks with similar intensities. This means that both  $\text{LiBH}_4$  fractions are in contact and  $\text{BH}_4^-$  can pass over the interface between these fractions. The strong intensity of the cross-peaks suggests that the interfacial area between the  $\text{LiBH}_4$  fractions is substantial.

Figures S15 and S16 show exchange spectra of MI-MS-8 recorded at 10 and 50 °C, respectively, using exchange times



between 1 and 625 ms. At short exchange times  $\leq 5$  ms, the peaks on the diagonal dominate, indicating that little exchange has occurred during this time. At exchange times of 25 ms or longer, cross-peaks become apparent, indicating the exchange of  $\text{BH}_4^-$  ions between the fractions. The relative intensity of the cross-peaks, compared to the diagonal peaks, increases with increasing exchange time. At the longest exchange time (625 ms), the cross-peaks are comparable in magnitude to the narrow diagonal peak, suggesting that a large amount of the originally highly dynamic  $\text{BH}_4^-$  ions has moved to the less-dynamic fraction. Vice versa, a comparable amount of initially less-dynamic  $\text{BH}_4^-$  ions migrated to the highly dynamic phase. In this case, the mixing time substantially exceeds the exchange time, which is consequently estimated to be on the order of 0.1 s. As the experiments are conducted at MAS spinning frequencies up to 40 kHz, spin diffusion is thought to play a minor role in these experiments (*vide infra*).

Zou et al.<sup>60</sup> did not find a temperature dependence of an exchange process in  $\text{LiBH}_4$  in porous carbon, and the results presented here do not reveal a very clear correlation between temperature and exchange rate, either. However, as discussed before, the ratio of the fractions strongly depends on the temperature. This makes it difficult to establish the exchange rate as a function of temperature as this is counteracted by the change in the interfacial area between the fractions.

**Dynamics at the Interface.** A two-dimensional exchange experiment with a temperature jump was performed to study the exchange of  $\text{BH}_4^-$  ions between the nanoconfined  $\text{LiBH}_4$  fractions upon an increase in temperature. Figure 6 shows the pulse sequence and resulting  $^{11}\text{B}$  exchange spectrum. The temperature-jump experiment differs from regular exchange experiments (the previous section) by the presence of strong radio frequency irradiation during the mixing time  $\tau$ , causing dissipative heating of the sample. Consequently, the vertical axis (corresponding to time  $t_1$ , before heating) relates to the sample at a lower temperature than the horizontal axis (time  $t_2$ , after heating), i.e., this spectrum shows the transport of  $\text{BH}_4^-$  ions from one phase to the other during heating. At the end of the acquisition time, the rf-irradiation is switched off and the sample reverts to its initial state/temperature before the next scan is acquired.

In the spectrum (Figure 6a), the two  $^{11}\text{B}$  fractions on the diagonal axis are clearly visible. Unlike the regular exchange experiments described earlier, the off-diagonal peaks are not symmetric about the diagonal. Above the diagonal line, a sizable cross-peak can be observed, whereas the off-diagonal intensity below the diagonal is marginal. The cross-peak above the diagonal corresponds to borohydride ions that are in the less-dynamic fraction before heating but end up being part of the dynamic fraction upon heating of the sample during the exchange time.

Comparison of the spectrum before (vertical) and after (horizontal) heating suggests that between 1 and 3% of the spectral intensity is in the asymmetric cross-peak. Comparing this with the quantitative SPE  $^1\text{H}$  spectra (Figure 4) implies that the temperature increases by  $4 \pm 3$  °C during the heating time (assuming that a new equilibrium is rapidly established after the mixing time  $\tau$ ). It is clear that a significant amount of borohydride ions in the less-dynamic fraction becomes part of the dynamic fraction upon heating, whereas the reverse process is much less significant during sample heating.

This observation has two important consequences. First, it shows that the exchange process can be attributed to a

physical, temperature-induced, exchange process. If the process would instead be the result of energy transfer between nearby nuclear spins, a process known as spin diffusion,<sup>61</sup> it would have been independent of temperature and the spectrum would have been symmetric about the diagonal. Hence, this confirms the presence of the physical exchange of borohydride ions between the two fractions.

Second, this proves that the highly dynamic fraction grows at the expense of the less-dynamic fraction, as a function of temperature. This process is thus responsible for the change in the ratio of the two confined fractions as a function of temperature. The aforementioned apparent absence of temperature dependence for the exchange rate is speculated to originate from the decrease in the interface area between the fractions when the layer of highly mobile ions is larger, a distribution of activation energies for the exchange process, or a combination of both, effectively counteracting the expected Arrhenius behavior.

## DISCUSSION

From our experiments, a view on the complex composition and dynamics of  $\text{LiBH}_4$  nanoconfined in silica SBA-15 emerges. Both  $\text{Li}^+$  and  $\text{BH}_4^-$  ions are present in two distinct fractions with different mobilities at near-ambient temperatures. The ratios of the dynamic and less-dynamic fractions are, within error, identical at 30 °C in both  $^7\text{Li}$  and  $^1\text{H}$  spectra. At this temperature, there appears to be a highly dynamic  $\text{LiBH}_4$  fraction that displays rotational and translational motions for both borohydride ions and lithium ions and might therefore be considered an ionic liquid.

The less-dynamic fraction resembles bulk o- $\text{LiBH}_4$  below the phase transition temperature. Two-dimensional-exchange experiments reveal a continuous exchange process of  $\text{BH}_4^-$  ions between both  $\text{LiBH}_4$  fractions at a hundred milliseconds time scale, showing that the fractions are in intimate contact and that the interface between the two  $\text{LiBH}_4$  fractions is large. This is consistent with the core-shell model proposed by Shane and Verdal et al. for nanoconfined  $\text{LiBH}_4$ .<sup>23,24</sup>

An intriguing question is what causes this behavior of  $\text{LiBH}_4$  in the SBA-15 pores. A well-known model is the space charge model that has been proposed to describe the interface between electrolytes and insulators.<sup>4,62</sup> This model predicts that ions can either be attracted or repelled by the charges on the surface of an insulator (such as silica), thereby creating defects in the ionic lattice, with the number of defects reducing exponentially with the distance from the insulator. It is well known that ionic mobility is correlated with defect formation propagation. For example, Lee et al. calculated that, once defects are formed, the activation energy for  $\text{Li}^+$  hopping in the low-temperature phase of  $\text{LiBH}_4$  is comparable to that in the highly conductive high-temperature phase.<sup>63</sup> Furthermore, the space charge model has been proposed to account for an increased lithium-ion mobility in several lithium salt/oxide composite systems.<sup>20,64,65</sup> However, the dynamic phase in this system is so dynamic that it is not considered to have a clear lattice structure, so we cannot really speak of a space charge model, and given the distinct  $^{11}\text{B}$  and  $^6\text{Li}$  peaks, any intermediate species on the interface between the fractions are expected to be very short-lived on the NMR time scale. Nevertheless, a specific interaction with the silica wall can contribute to the observed highly dynamic phase with greatly enhanced ion mobility for both  $\text{Li}^+$  and  $\text{BH}_4^-$  in  $\text{LiBH}_4/\text{SiO}_2$  nanocomposites. Moreover, it should be considered that the

morphology of SBA-15 is very complex resulting from the corrugation of the pores.<sup>54</sup> This might interfere with the crystallization of  $\text{LiBH}_4$  at the silica surface. The observation of “unfreezable” interfacial layers is well known for molecular liquids at silica surfaces.<sup>66</sup> The effect of corrugation might also relate to the different behavior of the two fractions observed in MCM-41. In that study,<sup>17</sup> we observed increasing dynamics with increasing temperature, but the relative amount of the two fractions remained constant. It should be noted, however, that the pores in that study were also much narrower (1.9 nm) compared to this study. In any case, the exact nature of the interactions at the silica surface needs further investigation. Further away from the silica surface, in the core of the pores, the regular bulk  $\text{LiBH}_4$  is expected to persist; its phase transition temperature is lowered, however.

At elevated temperatures, above the phase transition observed in the DSC experiments, the  $^1\text{H}$  and  $^{11}\text{B}$  NMR spectra clearly show there are still two distinct fractions of  $\text{BH}_4^-$  ions in the confined  $\text{LiBH}_4$ . In the  $^{6,7}\text{Li}$  NMR spectra, however, we only observe a single lithium fraction. Even more intriguing is the fact that the quadrupolar  $^7\text{Li}$  line shape of these lithium ions differs from the well-known line shapes of both bulk o- and h- $\text{LiBH}_4$ . A possible explanation for the observation of these lithium line shapes would be that all of the nanoconfined  $\text{LiBH}_4$  is highly disordered, leading to a large distribution in quadrupolar interaction parameters, smearing out the features of the quadrupolar line shape. It is very unlikely, however, that this disorder would lead to lower quadrupolar coupling constants than the bulk material. Moreover, previous studies already showed that the nanoconfined  $\text{LiBH}_4$  does not show a long-range order.<sup>19</sup> An amorphous phase without local order is not expected to show distinct satellite transitions. In addition, it does not explain our observation of two well-defined, distinct  $\text{BH}_4^-$  fractions.

We confirm that the phase transition observed by DSC corresponds to the transition from o- $\text{LiBH}_4$  in the core of the pores to the high-temperature hexagonal phase h- $\text{LiBH}_4$ . As was described by Suwarno et al.<sup>19</sup> for nanoconfined  $\text{LiBH}_4$  in silica, this transition takes place at lower temperatures than in the bulk phase. Our  $^{11}\text{B}$  NMR spectra show that above the phase transition we still have two  $\text{LiBH}_4$  fractions in the pores of the silica: a core of h- $\text{LiBH}_4$  surrounded by highly dynamic amorphous  $\text{LiBH}_4$  displaying the rapid translational motion of both  $\text{BH}_4^-$  and  $\text{Li}^+$  ions. It is known that the lithium ions in hexagonal  $\text{LiBH}_4$  are highly mobile.<sup>8</sup> Combined with the fact that we observed  $\text{BH}_4^-$  exchange between the two  $\text{LiBH}_4$  fractions, we therefore conclude that  $\text{Li}^+$  ions are able to exchange rapidly between the highly dynamic phase and h- $\text{LiBH}_4$ . If this exchange is rapid enough, we will observe an averaged quadrupolar line shape because of the difference in quadrupolar interaction parameters for  $^7\text{Li}$  in the two phases ( $C_Q = 0$  vs 37 kHz).

To validate this hypothesis, we simulated  $^7\text{Li}$  line shapes for a system in which a fraction of the  $\text{Li}^+$  ions experience an environment similar to that in bulk h- $\text{LiBH}_4$  and the other fraction experiences no quadrupolar interaction because of the mobility and lack of well-defined lattice sites in the highly dynamic phase. Figure S17 shows the resulting line shapes for such a situation, as a function of the exchange rate between the two fractions. Although this is a simplified model, assuming a specific ratio between the two fractions and equal probability to exchange for any  $^7\text{Li}$  atom, it can clearly be seen that at exchange rates of  $10^2$ – $10^3$  kHz, line shapes appear that are

very similar to the experimentally observed line shapes for the nanocomposites.

In conclusion, Figure 7 schematically depicts the structure and translational mobilities of the ions in  $\text{LiBH}_4/\text{SiO}_2$

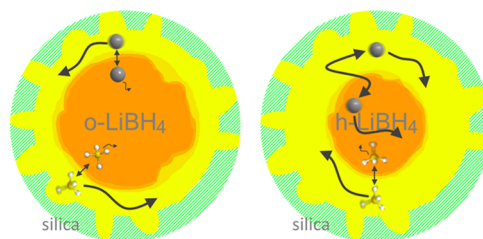


**Figure 7.** Model of nanoconfined  $\text{LiBH}_4$  showing the cross section of a single silica pore. The size of the arrows represents the time scales of the translational dynamics of  $\text{Li}^+$  and  $\text{BH}_4^-$  near ambient conditions (left) and above the temperature of the phase transition (right) in  $\text{LiBH}_4/\text{SiO}_2$  nanocomposites. Different colors are used to depict the dynamic and less-dynamic  $\text{LiBH}_4$  fractions for clarity.

nanocomposites at near-ambient and elevated temperatures, as discussed above. In the highly dynamic fraction near the pore walls, the translational mobility of the  $\text{Li}^+$  and  $\text{BH}_4^-$  ions is fast enough to average the NMR interactions, suggesting an ion hopping frequency above the 100 kHz time scale already at room temperature. In the core of the pores, the translational mobility of these ions is much slower, as is clear from the line shapes of tens of kilohertz wide for protons. The  $\text{BH}_4^-$  ions exchange over the border between the two fractions on a time scale on the order of 100 ms. The translational mobility of  $\text{Li}^+$  displays a similar trend as  $\text{BH}_4^-$  at room temperature. Lithium hopping is slow in the core of the pores, yet very fast motions are observed near the pore walls. Most likely, a slow exchange between the two  $\text{Li}^+$  fractions already occurs at ambient conditions, but this is difficult to study by NMR because the Li resonances of both phases overlap. However, above the phase transition of the  $\text{LiBH}_4$  in the core, the lithium mobility is very fast in both fractions, and exchange between these fractions occurs readily on the time scale of 0.1–1 MHz, as deduced from the observed  $^7\text{Li}$  quadrupolar line shapes.

Based on  $^1\text{H}$  exchange experiments, Zou et al. found a correlation time of 5 ms for the exchange process between the  $\text{BH}_4^-$  fractions for  $\text{LiBH}_4$  confined in carbon aerogels.<sup>60</sup> This is at least an order of magnitude shorter than for the  $\text{LiBH}_4/\text{SiO}_2$  nanocomposites studied here. An exchange time of 5 ms would lead to the coalescence of the separate resonances in the  $^{11}\text{B}$  spectra (Figure S12) for  $\text{BH}_4^-$  in the two fractions. This separation is about 1 ppm (270 Hz) at 20 T. It has been shown that the thickness of the layer of the highly dynamic  $\text{LiBH}_4$  depends on the support used.<sup>19</sup> Therefore, the differences in exchange times might result from different interactions of  $\text{LiBH}_4$  with different supports. This suggests that the interface properties of the support material play a major role in the lithium dynamics. However, effects of the pore structure cannot be excluded either, as the carbon support used by Zou et al. has a wide distribution in the pore diameter.

## CONCLUSIONS

We have studied the effect of nanoconfinement on the structure and dynamics of  $\text{LiBH}_4$ . Lithium borohydride confined in mesoporous silica was studied using solid-state NMR in the temperature range between room temperature



and 130 °C. This temperature range spans the range relevant for battery operation.

LiBH<sub>4</sub> in silica nanopores is clearly divided into two distinct fractions at all temperatures. One fraction is highly dynamic and lacks a clear structure over the entire temperature range, with both Li<sup>+</sup> and BH<sub>4</sub><sup>−</sup> diffusing rapidly through the material. The other fraction behaves similar to bulk LiBH<sub>4</sub>, except for its phase transition temperature. The relative abundance of the fractions suggests that the highly dynamic fraction resides near the silica pore walls, whereas the bulklike fraction is located in the core of the pores.

Spectra recorded at various temperatures revealed that the relative abundance of the dynamic fraction increases with temperature. Exchange experiments show that a continuous exchange of BH<sub>4</sub><sup>−</sup> ions between the fractions occurs on a 10–100 ms time scale. A temperature-jump exchange experiment proves that the interface between the fractions shifts as a function of temperature.

Near ambient temperatures, the translational motion of the Li<sup>+</sup> ions is similar to that of the BH<sub>4</sub><sup>−</sup> ions. In the dynamic fraction, the lithium ions are highly mobile, whereas Li<sup>+</sup> in the core fraction is less mobile, similar to that in the low-temperature phase of bulk LiBH<sub>4</sub>. Possibly, slow lithium exchange occurs between the fractions. Nevertheless, only a fraction of the Li<sup>+</sup> ions are mobile and potentially useful for battery applications under ambient conditions.

At elevated temperatures, when the phase transition of the bulklike confined material to the h-LiBH<sub>4</sub> structure has taken place, all Li<sup>+</sup> ions are highly mobile and readily cross the border between the two fractions on a microsecond time scale. Consequently, all lithium ions in the nanopores appear as a single, highly dynamic component in the NMR spectra.

For further optimization of LiBH<sub>4</sub>/SiO<sub>2</sub> (or complex metal hydrides on oxide hosts in general) for application in an all-solid-state battery, it is important that future work reveals the nature and thickness of the layer of highly mobile LiBH<sub>4</sub> and how this is influenced by the interaction with the silica pore walls for different types of silica. Only mobile ions contribute significantly to ionic conduction, and results so far suggest a strong dependence of the mobile layer thickness on the scaffold properties. The exact relation between the scaffold material and the dynamics of the ions needs further investigation.

## ■ ASSOCIATED CONTENT

### Supporting Information

The Supporting Information is available free of charge on the ACS Publications website at DOI: 10.1021/acs.jpcc.9b06477.

Characterization data (BJH pore size determination, DSC, and XRD) of the silica scaffolds and nanocomposites; additional <sup>67</sup>Li, <sup>11</sup>B, and <sup>1</sup>H NMR spectra; graphs of the line intensities as a function of temperature; and simulations of the effect of lithium exchange on the <sup>7</sup>Li NMR line shape (PDF)

## ■ AUTHOR INFORMATION

### Corresponding Author

\*E-mail: a.kentgens@nmr.ru.nl.

### ORCID

Peter Ngene: 0000-0003-3691-0623

Petra E. de Jongh: 0000-0002-2216-2620

Arno P. M. Kentgens: 0000-0001-5893-4488

## Notes

The authors declare no competing financial interest.

## ■ ACKNOWLEDGMENTS

The authors thank Hans Janssen, Gerrit Janssen, and Jan van Os for their technical support with the NMR experiments. Thijs Smolders and Fleur van Zelst are greatly acknowledged for performing supporting NMR experiments. Peter Bramwell is acknowledged for physisorption measurements. This project was supported by the Dutch Research Council (NWO), ECHO grant 712.015.005. NWO is further acknowledged for their support of the solid-state NMR facility for advanced materials science.

## ■ REFERENCES

- (1) Aurbach, D.; Zinigrad, E.; Cohen, Y.; Teller, H. A Short Review of Failure Mechanisms of Lithium Metal and Lithiated Graphite Anodes in Liquid Electrolyte Solutions. *Solid State Ionics* **2002**, *148*, 405–416.
- (2) Choi, N.-S.; Chen, Z.; Freunberger, S. A.; Ji, X.; Sun, Y.-K.; Amine, K.; Yushin, G.; Nazar, L. F.; Cho, J.; Bruce, P. G. Challenges Facing Lithium Batteries and Electrical Double-Layer Capacitors. *Angew. Chem., Int. Ed.* **2012**, *51*, 9994–10024.
- (3) Goodenough, J. B.; Park, K.-S. The Li-ion Rechargeable Battery: A Perspective. *J. Am. Chem. Soc.* **2013**, *135*, 1167–1176.
- (4) Chen, X.; Vereecken, P. M. Solid and Solid-Like Composite Electrolyte for Lithium Ion Batteries: Engineering the Ion Conductivity at Interfaces. *Adv. Mater. Interfaces* **2019**, *6*, No. 1800899.
- (5) Matsuo, M.; Orimo, S.-i. Lithium Fast-Ionic Conduction in Complex Hydrides: Review and Prospects. *Adv. Energy Mater.* **2011**, *1*, 161–172.
- (6) Unemoto, A.; Matsuo, M.; Orimo, S.-i. Complex Hydrides for Electrochemical Energy Storage. *Adv. Funct. Mater.* **2014**, *24*, 2267–2279.
- (7) Das, S.; Ngene, P.; Norby, P.; Vegge, T.; de Jongh, P. E.; Blanchard, D. All-Solid-State Lithium-Sulfur Battery Based on a Nanoconfined LiBH<sub>4</sub> Electrolyte. *J. Electrochem. Soc.* **2016**, *163*, A2029–A2034.
- (8) Matsuo, M.; Nakamori, Y.; Orimo, S.-i.; Maekawa, H.; Takamura, H. Lithium Superionic Conduction in Lithium Borohydride Accompanied by Structural Transition. *Appl. Phys. Lett.* **2007**, *91*, No. 224103.
- (9) Pistorius, C. W. F. T. Melting and Polymorphism of LiBH<sub>4</sub> to 45 kbar. *Z. Phys. Chem.* **1974**, *88*, 253–263.
- (10) Matsuo, M.; Takamura, H.; Maekawa, H.; Li, H.-W.; Orimo, S.-i. Stabilization of Lithium Superionic Conduction Phase and Enhancement of Conductivity of LiBH<sub>4</sub> by LiCl Addition. *Appl. Phys. Lett.* **2009**, *94*, No. 084103.
- (11) Matsuo, M.; Remhof, A.; Martelli, P.; Caputo, R.; Ernst, M.; Miura, Y.; Sato, T.; Oguchi, H.; Maekawa, H.; Takamura, H.; et al. Complex Hydrides with (BH<sub>4</sub>)<sup>−</sup> and (NH<sub>2</sub>)<sup>−</sup> Anions as New Lithium Fast-Ion Conductors. *J. Am. Chem. Soc.* **2009**, *131*, 16389–16391.
- (12) Maekawa, H.; Matsuo, M.; Takamura, H.; Ando, M.; Noda, Y.; Karahashi, T.; Orimo, S.-i. Halide-Stabilized LiBH<sub>4</sub>, a Room-Temperature Lithium Fast-Ion Conductor. *J. Am. Chem. Soc.* **2009**, *131*, 894–895.
- (13) Takano, A.; Oikawa, I.; Kamegawa, A.; Takamura, H. Enhancement of the Lithium-ion Conductivity of LiBH<sub>4</sub> by Hydration. *Solid State Ionics* **2016**, *285*, 47–50.
- (14) Zhan, L.; Zhang, Y.; Zhuang, X.; Fang, H.; Zhu, Y.; Guo, X.; Chen, J.; Wang, Z.; Li, L. Ionic Conductivities of Lithium Borohydride-Lithium Nitride Composites. *Solid State Ionics* **2017**, *304*, 150–155.
- (15) Gross, A. F.; Vajo, J. J.; Van Atta, S. L.; Olson, G. L. Enhanced Hydrogen Storage Kinetics of LiBH<sub>4</sub> in Nanoporous Carbon Scaffolds. *J. Phys. Chem. C* **2008**, *112*, 5651–5657.

- (16) Ngene, P.; Adelhelm, P.; Beale, A. M.; de Jong, K. P.; de Jongh, P. E. LiBH<sub>4</sub>/SBA-15 Nanocomposites Prepared by Melt Infiltration under Hydrogen Pressure: Synthesis and Hydrogen Sorption Properties. *J. Phys. Chem. C* **2010**, *114*, 6163–6168.
- (17) Verkuijlen, M. H. W.; Ngene, P.; de Kort, D. W.; Barré, C.; Nale, A.; van Eck, E. R. H.; van Bentum, P. J. M.; de Jongh, P. E.; Kentgens, A. P. M. Nanoconfined LiBH<sub>4</sub> and Enhanced Mobility of Li<sup>+</sup> and BH<sub>4</sub><sup>−</sup> Studied by Solid-State NMR. *J. Phys. Chem. C* **2012**, *116*, 22169–22178.
- (18) Blanchard, D.; Nale, A.; Sveinbjörnsson, D.; Eggenhuisen, T. M.; Verkuijlen, M. H. W.; Suwarno; Vegge, T.; Kentgens, A. P. M.; de Jongh, P. E. Nanoconfined LiBH<sub>4</sub> as a Fast Lithium Ion Conductor. *Adv. Funct. Mater.* **2015**, *25*, 184–192.
- (19) Suwarno; Ngene, P.; Nale, A.; Eggenhuisen, T. M.; Oschatz, M.; Embs, J. P.; Remhof, A.; de Jongh, P. E. J. Confinement Effects for Lithium Borohydride: Comparing Silica and Carbon Scaffolds. *J. Phys. Chem. C* **2017**, *121*, 4197–4205.
- (20) Choi, Y. S.; Lee, Y.-S.; Choi, D.-J.; Chae, K. H.; Oh, K. H.; Cho, Y. W. Enhanced Li Ion Conductivity in LiBH<sub>4</sub>-Al<sub>2</sub>O<sub>3</sub> Mixture via Interface Engineering. *J. Phys. Chem. C* **2017**, *121*, 26209–26215.
- (21) Lefevr, J.; Cervini, L.; Griffin, J. M.; Blanchard, D. Lithium Conductivity and Ions Dynamics in LiBH<sub>4</sub>/SiO<sub>2</sub> Solid Electrolytes Studied by Solid-State NMR and Quasi-Elastic Neutron Scattering and Applied in Lithium-Sulfur Batteries. *J. Phys. Chem. C* **2018**, *122*, 15264–15275.
- (22) Latroche, M.; Blanchard, D.; Cuevas, F.; El Kharbachi, A.; Hauback, B. C.; Jensen, T. R.; de Jongh, P. E.; Kim, S.; Nazer, N. S.; Ngene, P.; et al. Full-Cell Hydride-Based Solid-State Li Batteries for Energy Storage. *Int. J. Hydrogen Energy* **2019**, *44*, 7875–7887.
- (23) Shane, D. T.; Corey, R. L.; McIntosh, C.; Rayhel, L. H.; Bowman, R. C.; Vajo, J. J.; Gross, A. F.; Conradi, M. S. LiBH<sub>4</sub> in Carbon Aerogel Nanoscaffolds: An NMR Study of Atomic Motions. *J. Phys. Chem. C* **2010**, *114*, 4008–4014.
- (24) Verdal, N.; Udovic, T. J.; Rush, J. J.; Liu, X.; Majzoub, E. H.; Vajo, J. J.; Gross, A. F. Dynamical Perturbations of Tetrahydroborate Anions in LiBH<sub>4</sub> due to Nanoconfinement in Controlled-Pore Carbon Scaffolds. *J. Phys. Chem. C* **2013**, *117*, 17983–17995.
- (25) Chandran, C. V.; Heitjans, P. *Annual Reports on NMR Spectroscopy*; Academic Press, 2016; Vol. 89, Chapter 1, pp 1–102.
- (26) Eggenhuisen, T. M.; den Breejen, J. P.; Verdoes, D.; de Jongh, P. E.; de Jong, K. P. Fundamentals of Melt Infiltration for the Preparation of Supported Metal Catalysts. The Case of Co/SiO<sub>2</sub> for Fischer-Tropsch Synthesis. *J. Am. Chem. Soc.* **2010**, *132*, 18318–18325.
- (27) Galarneau, A.; Cambon, H.; Di Renzo, F.; Fajula, F. True Microporosity and Surface Area of Mesoporous SBA-15 Silicas as a Function of Synthesis Temperature. *Langmuir* **2001**, *17*, 8328–8335.
- (28) Brunauer, S.; Emmett, P. H.; Teller, E. Adsorption of Gases in Multimolecular Layers. *J. Am. Chem. Soc.* **1938**, *60*, 309–319.
- (29) Barrett, E. P.; Joyner, L. G.; Halenda, P. P. The Determination of Pore Volume and Area Distributions in Porous Substances. I. Computations from Nitrogen Isotherms. *J. Am. Chem. Soc.* **1951**, *73*, 373–380.
- (30) Jaroniec, M.; Kruk, M.; Olivier, J. P.; Koch, S. In *Characterisation of Porous Solids V*; Unger, K. K., Kreysa, G., Baselt, J., Eds.; Studies in Surface Science and Catalysis; Elsevier, 2000; Vol. 128, pp 71–80.
- (31) Jura, G.; Harkins, W. D. A New Adsorption Isotherm Which Is Valid Over a Very Wide Range of Pressure. *J. Chem. Phys.* **1943**, *11*, 430–431.
- (32) Ojeda, M. L.; Marcos Esparza, J.; Campero, A.; Cordero, S.; Kornhauser, I.; Rojas, F. On Comparing BJH and NLDFT Pore-Size Distributions Determined from N<sub>2</sub> Sorption on SBA-15 Substrata. *Phys. Chem. Chem. Phys.* **2003**, *5*, 1859–1866.
- (33) Ravikovitch, P. I.; Wei, D.; Chueh, W. T.; Haller, G. L.; Neimark, A. V. Evaluation of Pore Structure Parameters of MCM-41 Catalyst Supports and Catalysts by Means of Nitrogen and Argon Adsorption. *J. Phys. Chem. B* **1997**, *101*, 3671–3679.
- (34) Ammann, C.; Meier, P.; Merbach, A. E. A Simple Multinuclear NMR Thermometer. *J. Magn. Reson.* (1969) **1982**, *46*, 319–321.
- (35) Kaplan, M. L.; Bovey, F. A.; Cheng, H. N. Simplified Method of Calibrating Thermometric Nuclear Magnetic Resonance Standards. *Anal. Chem.* **1975**, *47*, 1703–1705.
- (36) Dybowski, C.; Neue, G. Solid State <sup>207</sup>Pb NMR Spectroscopy. *Prog. Nucl. Magn. Reson. Spectrosc.* **2002**, *41*, 153–170.
- (37) Bielecki, A.; Burum, D. P. Temperature Dependence of <sup>207</sup>Pb MAS Spectra of Solid Lead Nitrate. An Accurate, Sensitive Thermometer for Variable-Temperature MAS. *J. Magn. Reson., Ser A* **1995**, *116*, 215–220.
- (38) Hronský, V. Measurement of Sample Temperatures and Temperature Gradients in Magic-Angle Spinning NMR. *Acta Electrotech. Inf.* **2013**, *13*, 95–98.
- (39) Fenzke, D.; Freude, D.; Fröhlich, T.; Haase, J. NMR Intensity Measurements of Half-Integer Quadrupole Nuclei. *Chem. Phys. Lett.* **1984**, *111*, 171–175.
- (40) Solomon, I. Multiple Echoes in Solids. *Phys. Rev.* **1958**, *110*, 61–65.
- (41) Fung, B.; Khitrin, A.; Ermolaev, K. An Improved Broadband Decoupling Sequence for Liquid Crystals and Solids. *J. Magn. Reson.* **2000**, *142*, 97–101.
- (42) Markley, J. L.; Horsley, W. J.; Klein, M. P. Spin-Lattice Relaxation Measurements in Slowly Relaxing Complex Spectra. *J. Chem. Phys.* **1971**, *55*, 3604–3605.
- (43) Szeverenyi, N. M.; Sullivan, M. J.; Maciel, G. E. Observation of Spin Exchange by Two-Dimensional Fourier Transform <sup>13</sup>C Cross Polarization - Magic-Angle Spinning. *J. Magn. Reson.* (1969) **1982**, *47*, 462–475.
- (44) Schmidt-Rohr, K.; Clauss, J.; Spiess, H. W. Correlation of Structure, Mobility, and Morphological Information in Heterogeneous Polymer Materials by Two-Dimensional Wideline-Separation NMR Spectroscopy. *Macromolecules* **1992**, *25*, 3273–3277.
- (45) d'Espinose de Lacaillerie, J.-B.; Jarry, B.; Pascui, O.; Reichert, D. "Cooking the Sample": Radiofrequency Induced Heating During Solid-State NMR Experiments. *Solid State Nucl. Magn. Reson.* **2005**, *28*, 225–232.
- (46) van Beek, J. D. matNMR: A Flexible Toolbox for Processing, Analyzing and Visualizing Magnetic Resonance Data in Matlab. *J. Magn. Reson.* **2007**, *187*, 19–26.
- (47) Harris, R. K.; Becker, E. D.; Cabral De Menezes, S. M.; Goodfellow, R.; Granger, P. NMR Nomenclature. Nuclear Spin Properties and Conventions for Chemical Shifts (IUPAC Recommendations 2001). *Pure Appl. Chem.* **2001**, *73*, 1795–1818.
- (48) Morcombe, C. R.; Zilm, K. W. Chemical Shift Referencing in MAS Solid State NMR. *J. Magn. Reson.* **2003**, *162*, 479–486.
- (49) Lin, Y.-Y.; Hodgkinson, P.; Ernst, M.; Pines, A. A Novel Detection–Estimation Scheme for Noisy NMR Signals: Applications to Delayed Acquisition Data. *J. Magn. Reson.* **1997**, *128*, 30–41.
- (50) Bak, M.; Rasmussen, J. T.; Nielsen, N. C. SIMPSON: A General Simulation Program for Solid-State NMR Spectroscopy. *J. Magn. Reson.* **2000**, *147*, 296–330.
- (51) Arnbjerg, L. M.; Ravnsbæk, D. B.; Filinchuk, Y.; Vang, R. T.; Cerenius, Y.; Besenbacher, F.; Jørgensen, J.-E.; Jakobsen, H. J.; Jensen, T. R. Structure and Dynamics for LiBH<sub>4</sub>-LiCl Solid Solutions. *Chem. Mater.* **2009**, *21*, 5772–5782.
- (52) Epp, V.; Wilkening, M. Fast Li Diffusion in Crystalline LiBH<sub>4</sub> due to Reduced Dimensionality: Frequency-Dependent NMR Spectroscopy. *Phys. Rev. B* **2010**, *82*, No. 020301.
- (53) Liu, X.; Peaslee, D.; Jost, C. Z.; Baumann, T. F.; Majzoub, E. H. Systematic Pore-Size Effects of Nanoconfinement of LiBH<sub>4</sub>: Elimination of Diborane Release and Tunable Behavior for Hydrogen Storage Applications. *Chem. Mater.* **2011**, *23*, 1331–1336.
- (54) Gommès, C. J.; Friedrich, H.; Wolters, M.; de Jongh, P. E.; de Jong, K. P. Quantitative Characterization of Pore Corrugation in Ordered Mesoporous Materials Using Image Analysis of Electron Tomograms. *Chem. Mater.* **2009**, *21*, 1311–1317.
- (55) Van Vleck, J. H. The Dipolar Broadening of Magnetic Resonance Lines in Crystals. *Phys. Rev.* **1948**, *74*, 1168–1183.

- (56) Jimura, K.; Hayashi, S. Reorientational Motion of  $\text{BH}_4$  Ions in Alkali Borohydrides  $\text{MBH}_4$  ( $\text{M} = \text{Li}, \text{Na}, \text{K}$ ) as Studied by Solid-State NMR. *J. Phys. Chem. C* **2012**, *116*, 4883–4891.
- (57) Corey, R. L.; Shane, D. T.; Bowman, R. C.; Conradi, M. S. Atomic Motions in  $\text{LiBH}_4$  by NMR. *J. Phys. Chem. C* **2008**, *112*, 18706–18710.
- (58) Man, P. P. In *Encyclopedia of Analytical Chemistry*; Meyers, R. A., Dybowski, C., Eds.; John Wiley & Sons, Ltd., 2006; pp 12224–12265.
- (59) Łodziana, Z.; Błoński, P. Structure of Nanoconfined  $\text{LiBH}_4$  from First Principles  $^{11}\text{B}$  NMR Chemical Shifts Calculations. *Int. J. Hydrogen Energy* **2014**, *39*, 9842–9847.
- (60) Zou, H.; Gradišek, A.; Emery, S. B.; Vajo, J. J.; Conradi, M. S.  $\text{LiBH}_4$  in Aerogel: Ionic Motions by NMR. *J. Phys. Chem. C* **2017**, *121*, 15114–15119.
- (61) Bloembergen, N. On the Interaction of Nuclear Spins in a Crystalline Lattice. *Physica* **1949**, *15*, 386–426.
- (62) Maier, J. Space Charge Regions in Solid Two-Phase Systems and Their Conduction Contribution-I. Conductance Enhancement in the System Ionic Conductor-‘Inert’ Phase and Application on  $\text{AgCl}:\text{Al}_2\text{O}_3$  and  $\text{AgCl}:\text{SiO}_2$ . *J. Phys. Chem. Solids* **1985**, *46*, 309–320.
- (63) Lee, Y.-S.; Cho, Y. W. Fast Lithium Ion Migration in Room Temperature  $\text{LiBH}_4$ . *J. Phys. Chem. C* **2017**, *121*, 17773–17779.
- (64) Nakamura, O.; Goodenough, J. B. Conductivity Enhancement of Lithium Bromide Monohydrate by  $\text{Al}_2\text{O}_3$  Particles. *Solid State Ionics* **1982**, *7*, 119–123.
- (65) Maekawa, H.; Fujimaki, Y.; Shen, H.; Kawamura, J.; Yamamura, T. Mesopore Size Dependence of the Ionic Diffusivity in Alumina Based Composite Lithium Ionic Conductors. *Solid State Ionics* **2006**, *177*, 2711–2714.
- (66) Jähnert, S.; Vaca Chávez, F.; Schaumann, G. E.; Schreiber, A.; Schönhoff, M.; Findenegg, G. H. Melting and Freezing of Water in Cylindrical Silica Nanopores. *Phys. Chem. Chem. Phys.* **2008**, *10*, 6039–6051.